Desalination and Water Treatment
www.deswater.com

doi: 10.5004/dwt.2021.27629

234 (2021) 324–332
September

Expanded graphite-based membrane for water desalination

Vu T. Tan*, Hoang Thi Chien, La The Vinh

School of Chemical Engineering, Hanoi University of Science and Technology, No. 1 Dai Co Viet, Hanoi, Vietnam, email: tan.vuthi@hust.edu.vn (V.T. Tan)

Received 17 February 2021; Accepted 17 July 2021

ABSTRACT

For the first time, the expanded graphite (EG) was used as membrane-based for the desalination application. The EG is fabricated at room temperature using the optimizing weight ratio between ammonium persulfate and sulfuric acid. The highest expansion grade is 241 mL g^{-1} which is corresponded to the graphite with 305 μm of size, and the ratio between salt $(NH_4)_2S_2O_8$ and acid H_2SO_4 is 5:4. The conductivity of the filtered salt solution is 0.35 mS cm^{-1}, demonstrating two conductivity orders inferior to the initial salt solution 0.5 M (17.7 mS cm^{-1}). Besides, the filtered salt solution conductivity is located in the standard range of tap water. The salt removal capacity of EG is 9.32 mg g^{-1} (after filtering 500 mL of NaCl 0.5 M). This desalination capacity is lower than that of the 3D graphene-based membrane reported in the literature, 71.4 mg g^{-1} [1]. However, it is necessary to point out the preparation cost of EG is negligible compared with the cost preparation of 3D graphene membrane. Still, it is relatively higher than other desalination-based membranes reported in the literature, such as activated carbon, 2–5 mg g^{-1} [2]. The desalination result can be explained by the 2-dimensional structure of EG, which can provide an excellent molecular and ionic sieving effect. However, the EG exhibits low desalination stability due to the swell effect when it is contacted to an aqueous solution.

Keywords: Expanded graphite; Porous; Desalination; Membrane

1. Introduction

Recently, freshwater is a significant demand for human beings [3]. The desalination process to alleviate the water conflict could be a solution for today to solve this problem. However, the main problem is the energy required for the desalination purpose. Salt has a very high solubility in water, forming ionic bonding, which is very difficult to be broken. In addition, the recent desalination technologies are costly, making desalinating water upraised [3,4].

Among several standard techniques used for the desalination process, reverse osmosis is widely applied due to its effectiveness [5,6]. However, the technology involves a high installation cost, requires elevated energy consumption, and displays a small desalination capacity. Besides, fouling issues, rapid degradation, poor stability under corrosive ambient, and low fluidity because of the high pressure always are problematic for desalination membrane techniques [7,8]. Therefore, it is essential to develop a novel material used in desalination membranes to suppress those problems.

At the recent time, nanostructured carbon materials are popularly used in many industrial applications because of their outstanding properties such as chemically inert, elevated specific surface area, low-cost production [9–12]. It is already known that 2D materials, for example, graphene-based materials, provide an ideal approach for water-based filtration due to their layered structure [13]. Many researchers have demonstrated that the laminar structure may create nanocapillary channels, making a versatile way for solvent transport and improving ion rejection [14,15]. In addition, it was showed that the laminar structure membrane

* Corresponding author.

displays higher water flux and ionic rejection selectivity than polymeric-based membranes [16,17].

However, among the 2D graphene membrane, the graphene oxide (GO) membrane always suffers swelling problems due to its hydrophilic property [18]. The GO-based membrane also presents low stability when it is exposed to the aqueous solution [19]. The high-cost production of GO material may affect the use of the GO-based membrane. Aside from that, the desalination capacities of graphene material are pretty far from industrial applications [20,21].

Recently, other 2D nanomaterials, such as molybdenum disulfide (MoS_2) [22], phosphorene [23], boron nitride (BN) [24], and silicon carbide (SiC) [25] have been intensively developed in desalination applications. However, the desalination results were presented only using computational simulation and computational fluid dynamics calculation. Also, the manufacturing routes of those 2D nanomaterials are entirely complicated and lead to a high manufacturing cost [26]. Therefore, the use of the mentioned 2D nanomaterial in practical membrane desalination is still challenging.

Newly, expanded graphite (EG) is a 2D nanostructured modified graphite with an expansion degree of two graphite layers [27]. Its specific surface area is higher than that of initial graphite, leading to pores forming, making it a good absorbed material. Recently, EG has been commonly used to remove oil in the oil-water mixture, waste gas capture, organic dye removal, and several industrial applications due to its excellent absorption property [27–31]. However, to our best knowledge, EG is not popularly used in desalination seawater.

A new material based on EG was developed for water desalination application in this work, taking its excellent absorption property. The desalination results were quite surprising for the use of EG as a membrane-based material. On the other way, the EG fabrication cost is comparatively lower than other 2D desalination membrane materials. Thus, this research may open a new approach for the manufacturing of low-cost desalination membrane material.

2. Experimental

2.1. Preparation of EG

Natural graphite (NG) was collected from Bao Ha Mining, located in the Lao Cai Province in Vietnam, with a carbon content ≥ of 80%. The impurities of NG were removed by HCl 20% for several cycles. The cleaned NG has a carbon content >97%.

The fabrication of EG was performed at room temperature following Liu et al. [32]. However, in this work, the EG expansion degree was also studied by varying the reagent stoichiometries, expansion time, and graphite flake size:

- A mixture containing $(NH_4)_2S_2O_8$ and concentrated H_2SO_4 (95%) with different weight ratios was mechanically stirred for 10 min.
- 1 g of NG was gradually added into the prepared mixture and stirred for 5 min at room temperature; a slurry comprised of $(NH_4)_2S_2O_8$, H_2SO_4 and NG is obtained. After that, the slurry was translated to a watch glass for the completed expansion.
- The EG is neutralized by deionized water to pH neutral.

2.2. Desalination system

A simple filtration system contains a vertical filtration column and a collecting vessel (Fig. 1). The desalination membrane consists of 15 g of EG with an apparent density of 0.09 g cm^{-3}. The filtration process is performed at room temperature and under atmospheric pressure. The solution flow rate is 0.7 L cm^{-2} h^{-1}. The desalination capacity was evaluated by measuring the conductivity of the 50 mL filtered solution. All the conductivity measurements are assessed by Thermo Scientific Eutech ELITEPCTS equipment.

2.3. Characterization of the samples

The X-ray diffraction (XRD) spectra were recorded on a Bruker D8 ADVANCE instrument operating at 40 kV and 40 mA using Cu Kα radiation (λ = 0.15406 nm). The morphology of the samples was examined by scanning electron microscopy (SEM, HITACHI S-4800 model). The Raman spectra were recorded on a Micro Raman spectrophotometer (JASCO Raman NRS-3000) using a 633 nm excited laser at room temperature.

All the N_2 isotherm results were obtained on a Micromeritics ASAP 2020 analyzer. The Brunauer–Emmett–Teller equation was used to evaluate the specific surface area of EG. The degasification condition was done at 150°C under the vacuum condition for 15 h before starting the measurement. The specific surface area was calculated by the adsorbed amount vs. the relative pressure (P/P_0 from 0 to 0.30). The pore size distributions were determined by using the Barrett–Joyner–Halenda (BJH) model.

3. Results and discussion

3.1. Optimization of the preparation EG

It is already known that the high EG expansion volume is the key to increasing the specific surface area, thus improving salt retention. For the elevated expansion efficiency, the EG synthesis conditions were performed by the orthogonal method [33]. The standard 3^4 orthogonal

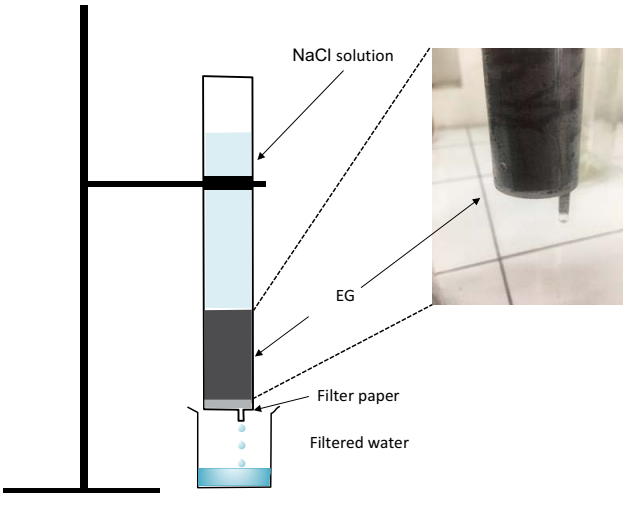

Fig. 1. The desalination system.

experimental condition design, the experimental factors, the expansion time, the stoichiometry of H_2SO_4 and $(NH_4)_2S_2O_8$, and graphite lateral size are listed in Table 1.

From the results in Table 1, the optimum conditions are obtained: 60 s of time synthesis, the weight stoichiometry between H_2SO_4 and $(NH_4)_2S_2O_8$ is 4:5, and the graphite lateral size is 305 μm. Therefore, the maximum expansion value is up to 241 mL g^{-1}. Thus, the EG prepared for further experiments will follow the mentioned preparation condition.

Recently, several works have reported that the weight loss of EG is closely correlated with its expansion degree due to the partial bunt at high temperature in the oven or the microwave. In our work, as the expansion temperature is at room temperature, no weight loss has been detected. The expansion mechanism can be explained as the following: in the time of expansion process, the persulfate anions react with sulfuric acid forming SO_2 and O_2 as the following reaction:

$$\left(NH_4\right)_2 S_2O_8 + 2H_2SO_4 \rightarrow H_2S_2O_8 + 2NH_4HSO_4 \quad \text{(A)}$$

$$H_2S_2O_8 \rightarrow H_2SO_4 + SO_2 + O_2 \quad \text{(B)}$$

The gases released can exert a force surpassing the Van der Waal force of graphite interlayers, separating two layers of graphite, resulting in the expansion process of graphite. Therefore, the expansion volume is affected principally by the gases emitted during the expansion process, which is strongly related to the weight ratios of $(NH_4)_2S_2O_8$ and H_2SO_4. Additionally, it can be seen that the expansion time has a slight effect on the expansion volume value.

The rapid decomposition of persulfate in sulfuric acid can describe the EG expansion at room temperature. However, it is necessary to point out that graphite particle size toughly influences the expansion volume. The expansion volume is increased when the particle size is enlarged, which is matched to many other results reported in the literature [34,35]. In our opinion, the influence of flake size can be clarified by the contact surface of graphite with the reaction mixture. The graphite with a large particle size has a vaster contact surface area than the small particle size. Thus, a massive amount of reaction mixture can distribute on the graphite layer and penetrated into the graphite interlayers, forming the expansion of graphite.

3.2. Characterization of the EG

3.2.1. SEM analysis

SEM characterization is a practical tool to study the material morphologies [36,37]. Fig. 2 shows the general morphologies of both graphite and EG. The graphite consists of large, platy, highly organized graphite crystals in the form of flakes. The layers of graphite seem compacted and present a smooth surface (Fig. 2a). The highly crystalline edge domain with minor matrix intercalation of the graphite can be clearly seen at the high magnification scale (Fig. 2b).

However, comparing with graphite, the morphology of EG is different. The original morphology was destroyed, and graphite was expanded along the *c*-axis under the persulfate decomposition, resulting in the fluffy worm-like structure at a low-magnification scale (Fig. 2c). The EG had superabundant pore networks at a high magnification scale, and a significant number of pores between the 1–2 μm range was clearly observed (Fig. 2d).

3.2.2. X-ray diffraction analysis

The XRD analysis was carried out in the range of the 2θ from 5° to 70°, as shown in Fig. 3a. The two strong peaks with the value of 26.7° (d_{002} = 0.333 nm) and 54.8° (d_{004} = 0.167 nm) are the main characteristic diffraction peaks of graphite. However, the EG diffraction peaks exhibited a significant reduction in intensity, making an increase in width at half maximum (FWHM) from 0.375 to 4.25 (Fig. 3b). During the expansion process, the partial destruction of crystal structure could clear up this change. The EG original structure layer was still conserved because of the non-oxidized graphite crystals, providing similar characteristic diffraction peaks between graphite and EG.

Table 2 shows the crystallographic parameters of graphite and EG. It can be noticed that during the expansion process, the value of d_{002} and L_c of EG compared with graphite are very similar. This result is because a small part of graphite was not expanded completely and retains the

Table 1
Experimental conditions of EG

Sample	Time, min	Dosage of H_2SO_4, g	Dosage of $(NH_4)_2S_2O_8$, g	Graphite lateral size, μm	Expansion volume, mL g^{-1}
1	30	3	5	75	140
2	30	4	4	125	198
3	30	5	3	305	196
4	**60**	**3**	**3**	**305**	**234**
5	60	4	4	75	145
6	60	5	5	125	189
7	90	3	3	125	187
8	**90**	**4**	**5**	**305**	**241**
9	90	5	4	75	143

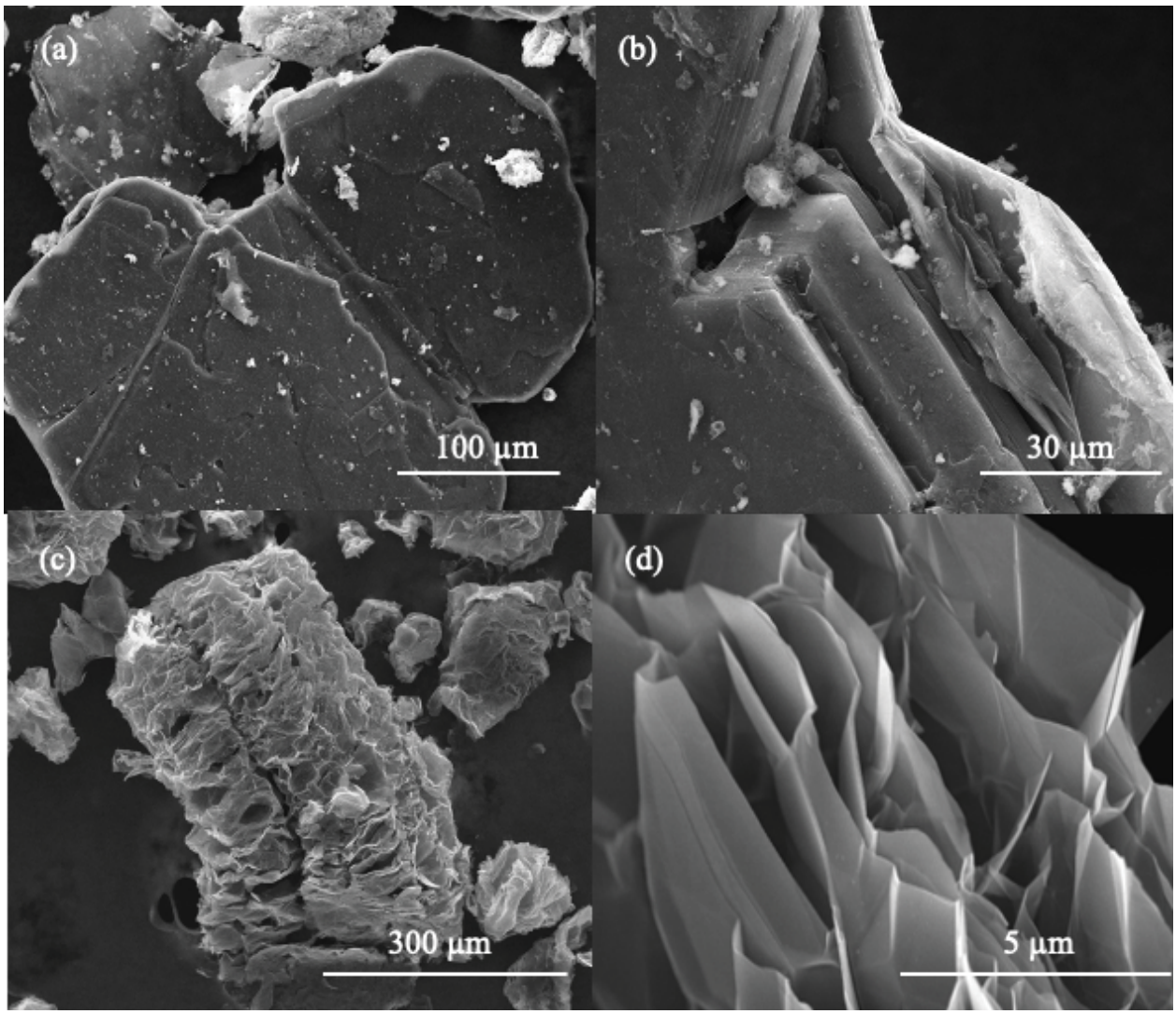

Fig. 2. SEM images of graphite (a,b) and EG (c,d).

original graphite structure. Also, L_a exhibited no noticeable changes in the a-axis direction, illustrating no effect of graphite lateral size.

3.2.3. Raman spectroscopy

Raman spectroscopy was applied to investigate the chemical structure, crystallinity, and molecular interactions of materials [38]. The Raman technique is used for graphite-based material to study the damage induced to graphite structure during the expansion process. As presented in Fig. 4, both graphite and EG samples contained a sharp G peak at 1,598 cm^{-1}, corresponding to the E2g vibration of sp^2-hybridized carbon atoms. The D peak associated with defects is absent in the graphite Raman spectrum, showing an orderly graphite structure. However, in the EG Raman spectrum, a weak D peak can be found around 1,358 cm^{-1}, associated with EG defects or disordered structure. Several researchers recently used the relative intensities ratio between D and G bands (I_D/I_G) to characterize the disorder degree of graphite. In this work, the ratio I_D/I_G of graphite and EG were 0 and 0.072, showing minor damage to the graphite structure during the expansion process.

3.2.4. N_2 adsorption/desorption measurement

For absorbing material, the specific surface area and pore size are critical parameters to evaluate their adsorption capacity. Fig. 5 exhibits N_2 adsorption/desorption curves of EG and graphite. Both of them are corresponded to type IV isotherm, but the isotherms of both materials are dissimilar. This difference can be described by the structure changing from the 2D dimensional shape of graphite to the 3D worm structure of EG. The isotherm of EG indicates the presence of mesopores, with a specific surface area of 26.02 $m^2\ g^{-1}$. Meanwhile, such parameter of graphite is 5.01 $m^2\ g^{-1}$. This specific surface area of EG shows that the material contains large pores. The result reveals the formation of the porous structure of EG after the expansion process.

Fig. 6 shows the Barret–Joyner–Halenda (BJH) pore size distributions of EG and graphite. No specific pore size can be found in the BJH of graphite. However, the BJH pore

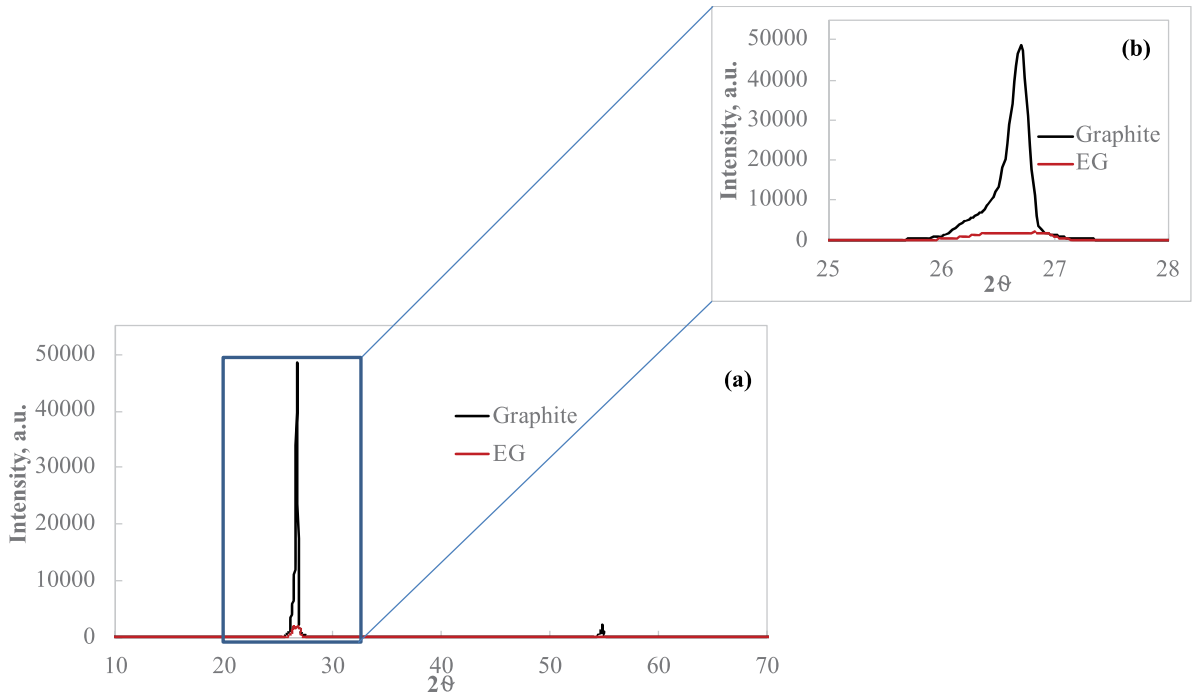

Fig. 3. XRD pattern of graphite (dark line) and EG (red line) (a); the high magnification of XRD pattern of graphite and EG from 25 to 28θ (b).

Table 2
Crystallographic parameters of graphite and EG

Samples	d_{002}/nm	$L_{a(110)}$/nm	$L_{c(002)}$/nm
Graphite	0.333	6.7	3.6
EG	0.364	7.1	3.9

Table 3
Elemental analysis of both simple graphite and EG by LECO combustion

Element, wt.%	Graphite	EG
C	99.6	98.5
O	0	0.3
S	0	0.6
H	0	0.1

size distribution of EG illustrates many mesoporous with the average pore sizes are 45 nm.

3.2.5. Elemental analysis

LECO combustion was used for the elemental analysis of EG and graphite. The carbon, hydrogen, sulfur, and oxygen content are determined through the pyrolysis and combustion process. The result reveals that graphite presents a 99.6% of carbon content; the 0.4% is related to the impurities of the graphite sample (Table 3). Compared with graphite, the EG has 98.5% carbon content; the amount of O, S and H could associate with the formed functional groups during the expansion.

3.3. Characterization of the filtered salt solution

The desalination efficiency of the synthesized EG was evaluated by the conductivity of the filtered solution passing through the filter system (Fig. 7).

Fig. 7 shows the conductivity performance of salt solution after going through the EG membrane-based system. The initial value conductivity of the prepared salt 0.5 M is 17.7 mS cm^{-1}, and the first filtration solution is 0.35 mS cm^{-1}. Therefore, the conductivity value is significantly reduced by almost two orders of magnitude after the first filtration. However, the conductivity became constant after filtration of a specific salt volume; the value stays in the range of 0.82–0.90 mS cm^{-1}. These filtration results can be described by the crystallization of NaCl salt in the interlayer distance of EG. This NaCl crystal may block the EG pore, leading to only a determined amount of salt passing the EG filter system and making the filtered solution conductivity constant.

The conductivity measurement of the filtered salt is in the range of two orders of magnitude lower than the initial salt solution. The filtered conductivity is also lower than 900 μS cm^{-1}, which locates in the acceptable region of the tap water. The stability of the filtration system was also checked by resining it with deionized water (Fig. 8).

The stability result presented in Fig. 8 shows that the EG membrane-based material shows a slight instability during the salt filtration process. The formation of NaCl crystals between the space of graphite layers could increase the distance between two graphite layers, providing the swell

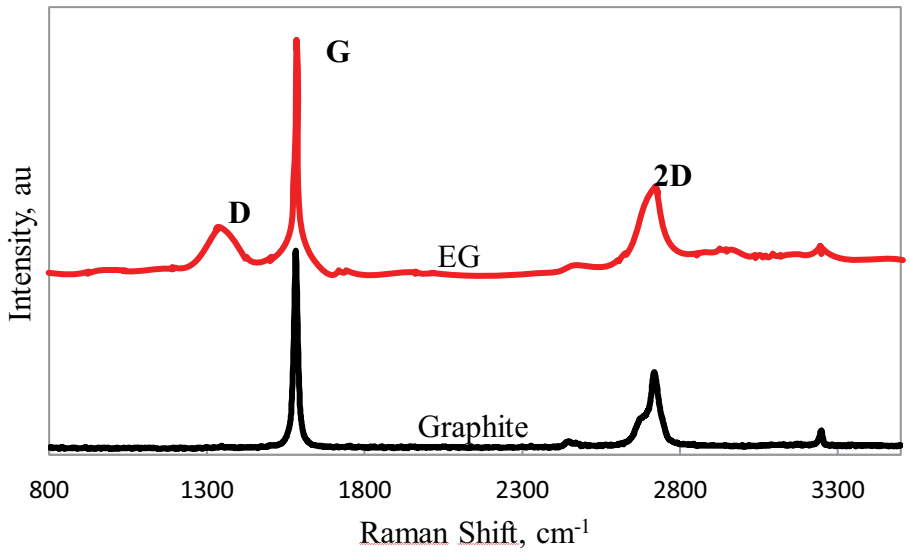

Fig. 4. Raman spectra of graphite (dark line) and EG (red line).

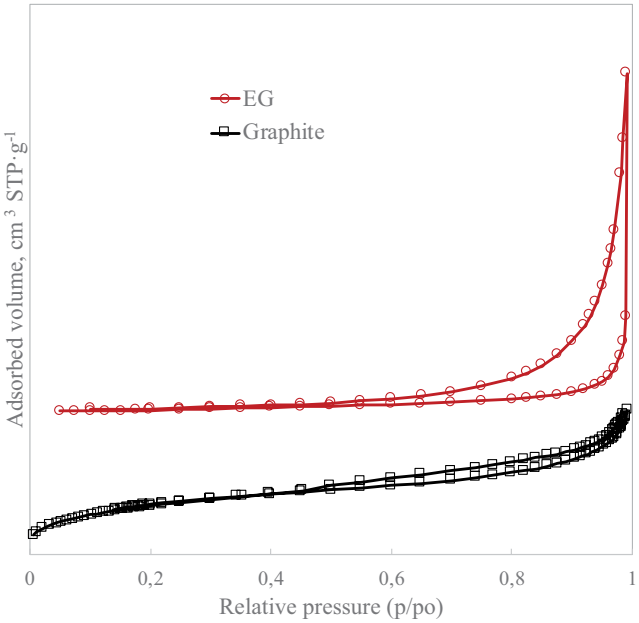

Fig. 5. N_2 adsorption–desorption curves of EG and graphite.

effect of EG. Thus, this phenomenon may decrease the salt rejection capacity of EG. In addition, further work will be performed to avoid the swelling effect and improve the EG membrane stability. The amount of salt eliminated from the salt solution was calculated by the following equation:

$$m = \int_0^V \left(C_0 - C_t\right) dV \quad (1)$$

where C_0 is the concentration of the fresh salt, C_t is the concentration of the filtered solution determined by the conductivity value, and V is the volume of the passed solution.

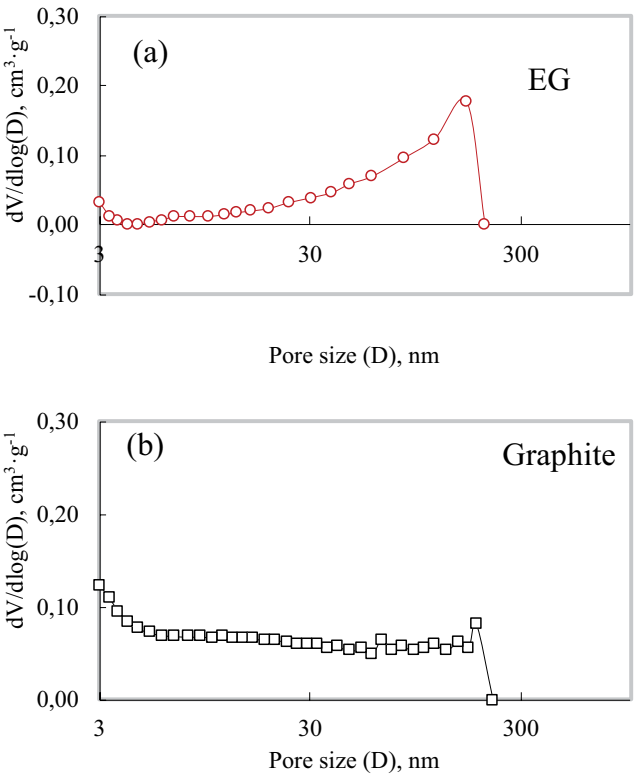

Fig. 6. Pore width distribution of graphite and EG.

The salt removal capacity of EG is 9.32 mg g^{-1} (after filtering 500 mL of NaCl 0.5 M). This result is lower than the capacity of graphene-based membrane [1,39], but considerably higher than that of activated carbon [2]. The EG cost production in this work is noticeably lower than the manufacturing cost of graphene-based material. Therefore, using EG for water desalination could be more economical than other high-cost 2D nanomaterials.

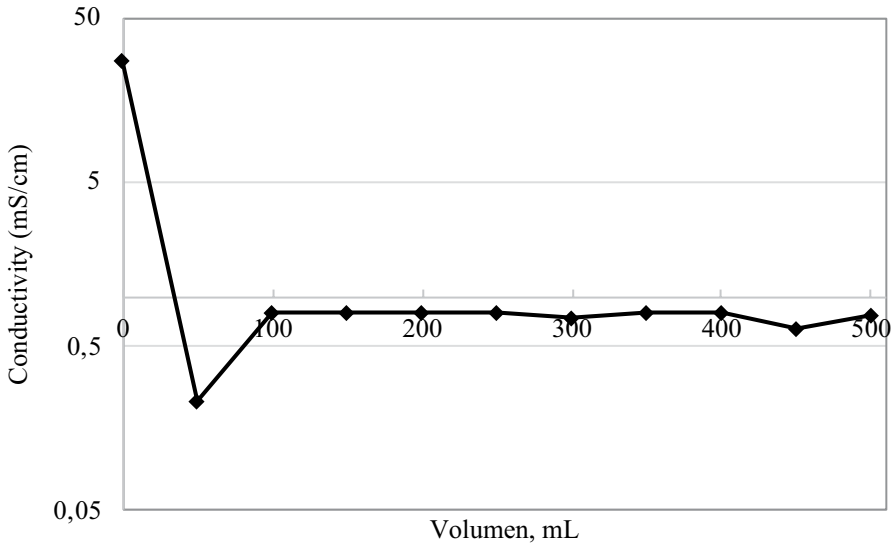

Fig. 7. Conductivity measurement of the filtered saltwater by filtering 0.5 M NaCl solution. The inset was plotted on a logarithmic scale.

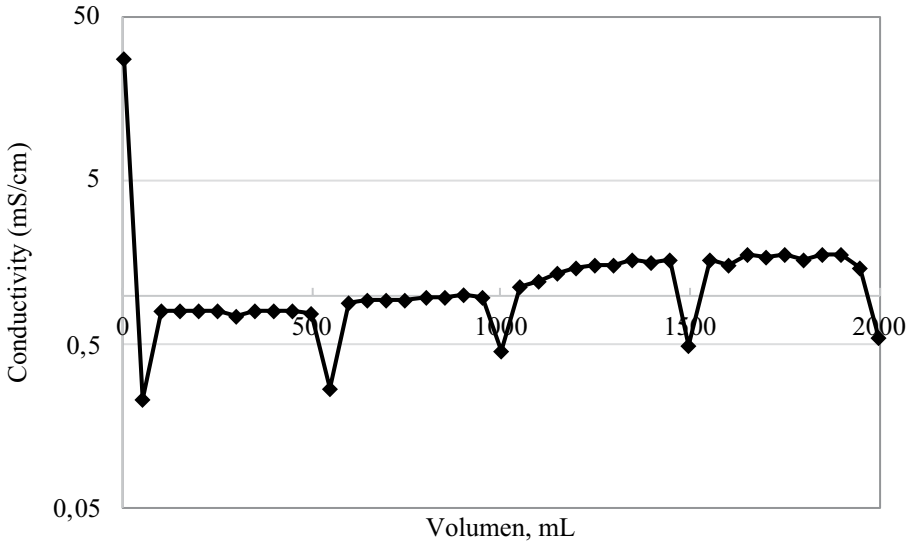

Fig. 8. Stability salt rejection of EG membrane-based material.

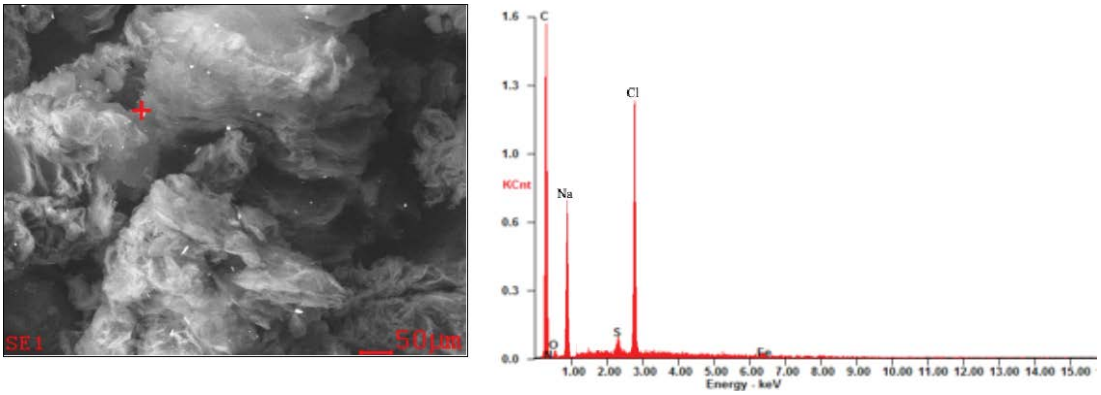

Fig. 9. EDX analysis of EG-based membranes after the filtration salt solution.

Fig. 9 shows the energy-dispersive X-ray spectroscopy (EDX) analysis of the EG-based membrane after the filtration of 0.5 M NaCl salt solution. The white salt crystals are attached to the interlayer of EG due to the NaCl crystal formation during the filtration process. The NaCl crystals are identified by EDX analysis of the EG-based membrane after passing the salt solution (EDX spectra).

4. Conclusions

For the first time, EG was used as a laminar membrane for desalination purposes. The synthesis parameters, such as expansion time, the dosage of H_2SO_4 and $(NH_4)_2S_2O_8$, graphite lateral size were varied by the orthogonal method to obtain the highest expansion grade.

The SEM characterization illustrated the fluffy worm-like structure of EG with a significant pore size between the 1–2 μm range. The XRD and Raman analysis show the disordered structure of the synthesized EG comparing with the original graphite.

The desalination results were significantly good. The treated solution has conductivity with two orders lower than the initial solution, and it stays in the tap water range. The desalination capacity of EG is lower than the graphene-based materials but higher than activated carbon. The low-cost production could make EG-based membranes are more economical than using another high production cost 2D nanomaterials. The study to avoid the swelling effect of EG and improve its stability will be established in the future work.

Acknowledgements

This research is funded by Vietnam Ministry of Education and Training under grant number B2020-BKA-562-22.

References

[1] T.T. Vu, T.C. Hoang, T.H.L. Vu, T.S. Huynh, T.V. La, Template-free fabrication strategies for 3D nanoporous graphene in desalination applications, Arabian J. Chem., 14 (2021) 103088–103099, doi: 10.1016/j.arabjc.2021.103088.
[2] A. Aghakhani, S.F. Mousavi, B. Mostafazadeh-Fard, R. Rostamian, M. Seraji, Application of some combined adsorbents to remove salinity parameters from drainage water, Desalination, 275 (2011) 217–223.
[3] N.C. Darre G. Toor, Desalination of water: a review, Curr. Pollut. Rep., 4 (2018) 1–8.
[4] Y. Ghalavand, M.S. Hatamipour, A. Rahimi, A review on energy consumption of desalination processes, Desal. Water Treat., 54 (2015) 1526–1541.
[5] G. Amy, N. Ghaffour, Z. Li, L. Francis, R.V. Linares, T. Missimer, S. Lattemann, Membrane-based seawater desalination: present and future prospects, Desalination, 401 (2016) 16–21.
[6] P.S. Goh, A.F. Ismail, A review on inorganic membranes for desalination and wastewater treatment, Desalination, 434 (2018) 60–80.
[7] C. Tan, O. Lefebvre, J. Zhang, H. Ng, S.-L. Ong, Membrane processes for desalination: overview, Membr. Technol. Environ. Appl., 34 (2012) 298–330.
[8] Y. Su, Chapter 1 – Current State-of-the-art Membrane Based Filtration and Separation Technologies, N.T.K Thanh, Ed., Graphene-Based Membranes for Mass Transport Applications, RSC Nanoscience and Nanotechnology, Cambrige, 2018, pp. 1–13.
[9] L. Borchardt, Q. Zhu, M.E. Casco, R. Berger, X. Zhuang, S. Kaskel, X. Feng Q. Xu, Toward a molecular design of porous carbon materials, Mater. Today, 20 (2017) 592–610.
[10] L.T. Vinh, T.N. Khiem, H.D. Chinh, P.V. Tuan, V.T. Tan, Adsorption capacities of reduced graphene oxide: effect of reductants, Mater. Res. Express, 6 (2019) 075615.
[11] T.P. Van, H. Trung, V. Tan, P. Tran, T.T.Q. Hoa, K. Tran, The dependence of morphology, structure, and photocatalytic activity of SnO_2/rGO nanocomposites on hydrothermal temperature, Mater. Res. Express, 6 (2019) 1–16.
[12] P. Van Tuan, T.T. Phuong, V.T. Tan, S.X. Nguyen, T.N. Khiem, In-situ hydrothermal fabrication and photocatalytic behavior of ZnO/reduced graphene oxide nanocomposites with varying graphene oxide concentrations, Mater. Sci. Semicond. Process., 115 (2020) 105114, doi: 10.1016/j.mssp.2020.105114.
[13] M. Hu B. Mi, Layer-by-layer assembly of graphene oxide membranes via electrostatic interaction, J. Membr. Sci., 469 (2014) 80–87.
[14] B. Chen, H. Jiang, X. Liu, X. Hu, Molecular insight into water desalination across multilayer graphene oxide membranes, ACS Appl. Mater. Interfaces, 9 (2017) 22826–22836.
[15] J. Lyu, X. Wen, U. Kumar, Y. You, V. Chen, R.K. Joshi, Separation and purification using GO and r-GO membranes, RSC Adv., 8 (2018) 23130–23151.
[16] P. Sun, K. Wang, H. Zhu, Recent developments in graphene-based membranes: structure, mass-transport mechanism and potential applications, Adv. Mater., 28 (2016) 2287–2310.
[17] J. Ma, D. Ping, X. Dong, Recent developments of graphene oxide-based membranes: a review, Membranes, 7 (2017) 1–29.
[18] S. Zheng, Q. Tu, J.J. Urban, S. Li, B. Mi, Swelling of graphene oxide membranes in aqueous solution: characterization of interlayer spacing and insight into water transport mechanisms, ACS Nano, 11 (2017) 6440–6450.
[19] S. Homaeigohar M. Elbahri, Graphene membranes for water desalination, NPG Asia Mater., 9 (2017) 1–16.
[20] W. Hirunpinyopas, E. Prestat, S.D. Worrall, S.J. Haigh, R.A.W. Dryfe, M.A. Bissett, Desalination and nanofiltration through functionalized laminar MoS_2 membranes, ACS Nano, 11 (2017) 11082–11090.
[21] A. Boretti, S. Al-Zubaidy, M. Vaclavikova, M. Al-Abri, S. Castelletto, S. Mikhalovsky, Outlook for graphene-based desalination membranes, npj Clean Water, 1 (2018) 1–16.
[22] M. Heiranian, A.B. Farimani, N.R. Aluru, Water desalination with a single-layer MoS_2 nanopore, Nat. Commun., 6 (2015) 8616, doi: 10.1038/ncomms9616.
[23] Y. Pathania, Gaganpreet, Self-passivated nanoporous phosphorene as a membrane for water desalination, Desalination, 497 (2021) 114777, doi: 10.1016/j.desal.2020.114777.
[24] L. Liang, J. Li, L. Zhang, Z. Zhang, J.W. Shen, L. Li, J. Wu, Computer simulation of water desalination through boron nitride nanotubes, Phys. Chem. Chem. Phys., 19 (2017) 30031–30038.
[25] A. Khataee, G. Bayat, J. Azamat, Molecular dynamics simulation of salt rejection through silicon carbide nanotubes as a nanostructure membrane, J. Mol. Graphics Modell., 71 (2017) 176–183.
[26] E.Y.M. Ang, T.Y. Ng, J. Yeo, R. Lin, Z. Liu, K.R. Geethalakshmi, Investigations on different two-dimensional materials as slit membranes for enhanced desalination, J. Membr. Sci., 598 (2020) 117653, doi: 10.1016/j.memsci.2019.117653.
[27] N.B. Hoang, T.T. Nguyen, T.S. Nguyen, T.P.Q. Bui, L.G. Bach, N.D. Duc, The application of expanded graphite fabricated by microwave method to eliminate organic dyes in aqueous solution, Cogent Eng., 6 (2019) 1584939.
[28] C. Xu, C. Jiao, R. Yao, A. Lin, W. Jiao, Adsorption and regeneration of expanded graphite modified by CTAB-KBr/H_3PO_4 for marine oil pollution, Environ. Pollut., 233 (2018) 194–200.
[29] Z. Hu, L. Cai, J. Liang, X. Guo, W. Li, Z. Huang, Green synthesis of expanded graphite/layered double hydroxides nanocomposites and their application in adsorption removal of Cr(VI) from aqueous solution, J. Cleaner Prod., 209 (2019) 1216–1227.
[30] T.A. Tabish, F.A. Memon, D.E. Gomez, D.W. Horsell, S. Zhang, A facile synthesis of porous graphene for efficient water and wastewater treatment, Sci. Rep., 8 (2018) 1–13.

[31] S. Tan, P. Shi, R. Su, M. Zhu, Removal of methylene blue from aqueous solution by powdered expanded graphite: adsorption isotherms and thermodynamics, Adv. Mater. Res., 424–425 (2012) 1313–1317.
[32] T. Liu, R. Zhang, X. Zhang, K. Liu, Y. Liu, P. Yan, One-step room-temperature preparation of expanded graphite, Carbon, 119 (2017) 544–547.
[33] X.-J. Yu, J. Wu, Q. Zhao, X.-W. Cheng, Preparation and characterization of sulfur-free exfoliated graphite with large exfoliated volume, Mater. Lett., 73 (2012) 11–13.
[34] Ö. Çalın, A. Kurt, Y. Celik, Influence of expansion conditions and precursor flake size on porous structure of expanded graphite, Fullerenes Nanotubes Carbon Nanostruct., 1 (2020) 611–620.
[35] C. Wang, H. Liu, C. Qin, S. Bi, Getting graphite nano-sheets with different sizes by choosing parent graphite: ultrasonication assisted preparation, IOP Conf. Ser.: Mater. Sci. Eng., 182 (2017) 012027.
[36] V.T. Tan, L. The Vinh, L. Tu Quynh, H. Thu Suong, H. Dang Chinh, A novel synthesis of nanoflower-like zinc borate from zinc oxide at room temperature, Mater. Res. Express, 7 (2020) 015059.
[37] V.T. Tan, L.T. Vinh, T.N. Khiem, H.D. Chinh, Facile template in-situ fabrication of $ZnCo_2O_4$ nanoparticles with highly photocatalytic activities under visible-light irradiation, Bull. Chem. React. Eng. Catal., 14 (2019) 404–412.
[38] V.T. Tan, L.T. Vinh, V.M. Khoi, H.D. Chinh, P.V. Tuan, T.N. Khiem, A new approach for the fabrication of tetragonal $BaTiO_3$ nanoparticles, J. Nanosci. Nanotechnol., 21 (2021) 2692–2701.
[39] P.B. Pawar, S. Saxena, D.K. Badhe, R.P. Chaudhary, S. Shukla, 3D oxidized graphene frameworks for efficient nano sieving, Sci. Rep., 6 (2016) 1–6.